INTERNATIONAL JOURNAL FOR NUMERICAL METHODS IN ENGINEERING
Int. J. Numer. Meth. Engng 2013; **93**:118–134
Published online 9 July 2012 in Wiley Online Library (wileyonlinelibrary.com). DOI: 10.1002/nme.4384

A new hole insertion method for level set based structural topology optimization

Peter D. Dunning and H. Alicia Kim*,†

Department of Mechanical Engineering, University of Bath, BA2 7AY, UK

SUMMARY

Structural shape and topology optimization using level set functions is becoming increasingly popular. However, traditional methods do not naturally allow for new hole creation and solutions can be dependent on the initial design. Various methods have been proposed that enable new hole insertion; however, the link between hole insertion and boundary optimization can be unclear. The new method presented in this paper utilizes a secondary level set function that represents a pseudo third dimension in two-dimensional problems to facilitate new hole insertion. The update of the secondary function is connected to the primary level set function forming a meaningful link between boundary optimization and hole creation. The performance of the method is investigated to identify suitable parameters that produce good solutions for a range of problems. Copyright © 2012 John Wiley & Sons, Ltd.

Received 15 March 2011; Revised 5 April 2012; Accepted 3 June 2012

KEY WORDS: topology optimization; level set method; hole insertion; compliance minimization

1. INTRODUCTION

Structural topology optimization aims to provide solutions that are independent of the initial design. This enables great potential for finding optimal designs with potentially novel configurations. The early approaches to topology optimization for continuum structures split the design domain into discrete elements [1, 2]. The design variables become the amount of material within each element, enabling dramatic changes in shape and topology. However, solutions produced by element-based methods often possess checkerboard patterns, which are regarded as numerical artifacts and not realistic arrangements of material [3, 4]. Various methods have been proposed to eliminate checkerboard patterns. However, solutions can depend on the introduction of additional constraints [5], computational cost is increased by using higher order elements [3, 4], or a heuristic sensitivity smoothing scheme is employed [6]. Another drawback of element-based methods is that solutions often contain 'fuzzy' unclear boundaries and require post processing to extract a practical design [7, 8].

Boundary-based methods are an alternative approach to topology optimization. This paradigm inherently produces designs with clearly defined boundaries and solutions do not possess checkerboard patterns [9]. The bubble method is a boundary-based topology optimization method that extends spline-based shape optimization by introducing a criterion to insert new holes [10]. However, shape optimization and hole insertion are performed consecutively. Thus, the bubble method is inefficient as a topology optimization method, because topology can only be changed after the shape of the current design has converged. Furthermore, topology optimization often involves large movement of boundaries and merging or splitting of holes. When using splines, special methods

*Correspondence to: H. Alicia Kim, Department of Mechanical Engineering, University of Bath, BA2 7AY, UK.
†E-mail: H.A.Kim@bath.ac.uk

are often required to split and merge holes [11]. Large boundary movement can cause control point bunching, or spreading, leading to a poorly represented boundary. An alternative method for boundary representation is to use a discretized implicit function. This naturally allows for complex topology changes and large boundary movements, without requiring special treatment or additional methods [12, 13].

The level set method is currently a popular method for optimizing structures defined by an implicit function. The level set method was originally developed as a flexible and robust computational tool to track the motion of interfaces [14, 15]. The direct approach to level set based structural optimization is to update the implicit function using a velocity function derived from shape sensitivity analysis, such that the design progresses iteratively towards an optimum [12, 13]. However, the direct level set optimization method cannot create new holes during optimization, at least for two-dimensional (2D) problems. This is a significant limitation for topology optimization, because the solution can be dependent on the initial design, or number of holes.

Various methods have been proposed to enable hole creation for the direct level set method. Topological derivatives are a popular mechanism for this, because they indicate the change in objective when a small hole is inserted into the design. Several methods have been proposed to introduce topological derivatives into the level set method. One approach is to add a forcing term to the implicit function update step, allowing new holes to emerge in favorable locations during optimization [16, 17]. However, the strength of the forcing term can affect efficiency and stability. Also, if the implicit function is initialized as a signed distance function, it is more difficult for holes to emerge further away from the boundary. Indeed, topological derivatives can be exclusively employed to update the implicit function, without considering shape derivatives [18, 19].

However, by far the most common approach is to create a small hole during optimization of the existing boundaries via the front-tracking algorithm. One approach is to use topological derivatives to indicate the locations of new holes after a number of boundary updates have been performed [20]. Noting that topological derivative is proportional to local strain energy, a similar hole creation approach has been presented where new holes are created in low strain energy regions at every specified number of iterations [21]. However, the number of iterations between hole creations is arbitrary and this can lead to a slow convergence and/or even suboptimal solutions. An alternative approach has been formulated where a hole is created in areas of low stress [22]. The adaptive inner front method creates holes by removing a specified volume of material, again with low strain energy [23]. Although these criteria of strain energy or stress offers a mechanism that is easy to understand in terms of where to create a hole, it is difficult to establish when it is more optimal to create a hole or to continue with boundary updates. Numerical parameter(s) is often introduced to control the hole creation but the selection of these values is usually problem dependent and arbitrary. This can result in a mismatch of optimalities between the existing boundaries and new holes and this inconsistency can lead to a suboptimal solution.

The level set optimization method proposed by Yamada *et al*. [24] allows holes to emerge during optimization. This method differs from the direct level set method in several ways. First, the implicit function is limited to be between -1 and $+1$. A fictitious interface energy term is added to objective function, which regularizes the optimization problem. Constraints are also added to the objective function using Lagrange multipliers. The Lagrangian is then optimized using derivatives that are equivalent to topological derivatives. The optimization of the Lagrangian replaces the traditional level set update equation that is used in the direct method. This approach allows holes to emerge during optimization, because the derivatives are equivalent to topological derivatives and the implicit function is updated over the entire domain, each step.

In the direct level set method, extension velocities are derived from shape sensitivities computed at the boundary of the structure. An alternative approach is to compute extension velocities over the entire domain from derivatives of a Lagrangian objective function [25]. These derivatives are physically meaningful because they are a measure of mutual energy density. The implicit function over the entire domain can then be updated each iteration. This allows holes to nucleate where the extension velocity is negative within the structure. However, the optimization problem is ill-posed, which can cause significant numerical instabilities. Therefore, a sensitivity filtering method is employed to smooth the extension velocity field and stabilize the method.

DOI: 10.1002/nme

The discretized implicit function can be approximated using radial basis functions (RBFs). The design variables become the expansion coefficients of the RBFs at each discrete point or node. If sensitivities are computed at each node then holes can emerge naturally when the coefficients are updated [26]. Holes can also emerge near the boundary in an RBF type approach if a volume integral method is used to compute shape sensitivities within a narrow band around the boundary [27]. The spectral level set method uses a finite Fourier series to reduce the number of design variables [28]. Design variables are the coefficients of the Fourier series that can be freely altered during optimization to change topology and introduce new holes. However, the topology and number of holes is restricted by the number of the function coefficients. The evolutionary structural optimization method has also been combined with the direct level set method to enable the creation of new holes [29]. The approach is to compute a performance index for each node based on the local values of strain energy. During the optimization, holes are created around a small number of nodes that have a low value of the performance index.

Despite the different level set and implicit function optimization approaches, the direct approach is still attractive, because there are robust and efficient numerical procedures readily available that have been developed for various applications of the level set method [14, 15]. However, most existing hole creation techniques for the direct method focus mainly on finding optimal locations to create new holes and do not consider whether creating a new hole is more beneficial than updating the boundary in that iteration. This is because there is no clear link between shape and topology optimization and holes are inserted at arbitrary times during the optimization. The need for a connection between shape and topological derivatives has also been recognized by other researchers, for example, [30].

This paper introduces a novel hole insertion technique for the direct level set based optimization method when solving two-dimensional problems. The method is derived from the observation that holes can be naturally created in three-dimensional (3D) problems by intersection of two approaching level set surfaces. Our approach utilizes this phenomenon by introducing a pseudo third dimension into the two-dimensional problem. The paper is organized as follows. First the direct level set structural optimization method is presented, including shape sensitivity analysis. Next, the details of our numerical implementation of the direct approach are presented. Then the new hole creation method is introduced, including its numerical implementation, followed by investigations of its performance using classic compliance minimization examples.

2. LEVEL-SET-BASED STRUCTURAL OPTIMIZATION

This section introduces the minimization of the compliance problem and briefly reviews how the problem can be solved using the level set method. First, the structure is defined by an implicit function $\phi(x)$, so that its zero level set coincides with the boundary:

$$\begin{cases} \phi(x) > 0, & x \in \Omega_S \\ \phi(x) = 0, & x \in \Gamma_S \\ \phi(x) < 0, & x \notin \Omega_S \end{cases} \tag{1}$$

where Ω_S is the domain of the structure and Γ_S is the boundary of the structure. The compliance of the structure, $C(u, \phi)$ is minimized subject to an upper limit on structural volume

$$\begin{aligned} &\text{Minimize: } C(u,\phi) = \int_\Omega E\varepsilon(u)\varepsilon(u)H(\phi)\mathrm{d}\Omega \\ &\text{Subject to: } \int_\Omega H(\phi)\mathrm{d}\Omega \leqslant Vol^* \\ &\qquad \int_\Omega E\varepsilon(u)\varepsilon(v)H(\phi)\mathrm{d}\Omega = \int_\Omega bvH(\phi)\mathrm{d}\Omega + \int_{\Gamma_S} fv\mathrm{d}\Gamma_S \\ &\qquad u|_{\Gamma_D} = 0 \quad \forall v \in U \end{aligned} \tag{2}$$

where Ω is a domain larger than Ω_S such that $\Omega_S \subset \Omega$, Vol^* is the limit on material volume, E is the material property tensor, $\varepsilon(u)$ the strain tensor under displacement field u, U is the space of

DOI: 10.1002/nme

kinematically permissible displacement fields, v is any permissible displacement field, b are body forces, f are surface tractions, and $H(\phi)$ is the Heaviside function

$$H(\phi) = \begin{cases} 1, & \phi \geqslant 0 \\ 0, & \phi < 0 \end{cases} \tag{3}$$

The key principle of level-set-based optimization is to use shape sensitivity analysis to define a velocity function that progresses the structure towards an optimum. This update process is usually performed by solving a Hamilton–Jacobi type equation

$$\frac{\partial \phi(x,t)}{\partial t} + \nabla \phi(x,t) \frac{\mathrm{d}x}{\mathrm{d}t} = 0 \tag{4}$$

where t acts as a fictitious time domain. Equation (4) can be discretized and rearranged to produce a convenient update formula for optimization

$$\phi_i^{k+1} = \phi_i^k - \Delta t \left| \nabla \phi_i^k \right| V_{n,i} \tag{5}$$

where $V_{n,i}$ is a discrete value of the velocity function acting normal to the boundary at point i, Δt is a discrete time step and k is the current iteration.

The shape derivative for the compliance objective function, Equation (2), is [13]

$$\begin{aligned} C'(u,\phi) = & \int_{\Gamma_\mathrm{N}} \left(E\varepsilon(u)\varepsilon(u) - 2\left[\frac{\partial (fu)}{\partial n} + \kappa(fu) + bu \right] \right) V_n \mathrm{d}\Gamma_\mathrm{N} \\ & - \int_{\Gamma_\mathrm{D}} E\varepsilon(u)\varepsilon(u) V_n \mathrm{d}\Gamma_\mathrm{D} \end{aligned}, \tag{6}$$

where V_n is a velocity function normal to boundary and a positive velocity moves the boundary inward, n is the unit normal vector, κ is the mean curvature and $\Gamma = \Gamma_\mathrm{N} \cup \Gamma_\mathrm{D}$. For practical reasons the portion of the boundary subject to surface tractions and displacement boundary conditions is often fixed during optimization. Therefore, the Γ_N part of the boundary is split so that $\Gamma_\mathrm{N} = \Gamma_\mathrm{F} \cup \Gamma_\mathbf{0}$, where Γ_F is the part subject to surface tractions and $\Gamma_\mathbf{0}$ the free part of the boundary that is permitted to move during optimization. To fix Γ_F and Γ_D during optimization, the velocity function is defined to be zero along those parts of the boundary. Under this condition, the shape derivative, Equation (6), simplifies to

$$C'(u,\phi) = \int_{\Gamma_\mathbf{0}} \left(E\varepsilon(u)\varepsilon(u) - 2bu \right) V_n \mathrm{d}\Gamma_\mathbf{0}. \tag{7}$$

The shape sensitivity, $\varsigma(u)$ of the compliance function along the free boundary is defined here as

$$\varsigma(u) = E\varepsilon(u)\varepsilon(u) - 2bu. \tag{8}$$

The goal of the optimization problem is to minimize the compliance function, Equation (2). Thus, the velocity function can be simply defined from the shape sensitivity to produce a negative sign of the shape derivative, Equation (7)

$$V_n = -\varsigma(u) = -E\varepsilon(u)\varepsilon(u) + 2bu. \tag{9}$$

The velocity function is then used to update the implicit function using Equation (5), thus improving the structure with respect to the objective. However, the velocity function does not account for the volume constraint. The most common approach to handle constraints is to transform the constrained problem into an unconstrained one using the Lagrange multiplier method. The unconstrained compliance problem is then

$$\text{Minimize:} \bar{C}(u,\phi) = \int_\Omega E\varepsilon(u)\varepsilon(u) H(\phi) \mathrm{d}\Omega + \lambda \int_\Omega H(\phi) \mathrm{d}\Omega \tag{10}$$

DOI: 10.1002/nme

where λ is a positive Lagrange multiplier. The shape derivative of the second part of the unconstrained problem can be easily evaluated and the shape derivative for Equation (10) is

$$\bar{C}'(u,\phi) = \int_{\Gamma_0} (\varsigma(u) - \lambda)\, V_n \mathrm{d}\Gamma_0. \tag{11}$$

Therefore, the velocity function can be simply redefined as

$$V_n = \lambda - \varsigma(u). \tag{12}$$

3. NUMERICAL IMPLEMENTATION

This section presents our numerical implementation of the direct level set method to solve the compliance problem, Equation (2). First the design domain is discretized using equal-sized square elements, with edge length h. The implicit function $\phi(x)$, Equation (1), is discretized at nodes of these elements and interpolated using bilinear shape functions. The initial values of $\phi(x)$ are defined as a signed distance function, such that their sign is defined by Equation (1) and their magnitude is equal to the distance from the grid node to the nearest boundary point. The elements are also used to perform the finite element analysis required to compute displacements and sensitivities. This fixed mesh approach to finite element analysis is popular in level set structural optimization because of its simplicity and efficiency compared with the fitted mesh approach. However, fixed elements can be intersected by the boundary.

A popular and efficient method to handle intersected elements is to approximate their stiffness using the area fraction of material within the element

$$K_\mathrm{A} = \frac{\alpha_\mathrm{A}}{\alpha_\mathrm{I}} K_\mathrm{I}, \tag{13}$$

where K_A is the stiffness matrix of an approximated element, K_I is the stiffness matrix of an element completely filled with material, α_I is the area of the complete element and α_A is the area of material within the approximated element. The elements used in our implementation are plane four-node bilinear elements [31]. However, the area fraction weighted fixed grid approach can have a destabilizing effect on optimization because of poor computation of boundary sensitivities [32–35]. Therefore, sensitivity computation is improved by employing a weighted least squares technique [36].

The time step in Equation (5) is constrained by the Courant–Friedrichs–Lewy condition for stability: $\Delta t = h/2|V_{n,i}|_{\max}$. The velocity function defined in Equation (12) is only applicable to the points along the boundary. To update the level set function using Equation (5), discrete velocity values, $V_{n,i}$, are required at all grid points. This is achieved using a velocity extension technique that extrapolates velocities away from the boundary [37]. This method ensures the preservation of the signed distance property by using the fast marching method to solve the following equation for extension velocities, V_ext:

$$\nabla\phi_\mathrm{temp}\nabla V_\mathrm{ext} = 0, \tag{14}$$

where ϕ_temp is a temporary signed distance implicit function. Preserving the signed distance property of the implicit function is desirable because it promotes stability in the level set method.

Further efficiency is gained by combining the extension velocity method with the narrow band approach, so that extension velocities are only computed within a local region around the boundary and not over the entire domain [38]. The extent of the narrow band region is called the bandwidth, ω. Extension velocities are only calculated for nodes that meet the criterion: $-\omega \leqslant \phi_i^0 \leqslant +\omega$, where ϕ_i^0 is the initial value of the signed distance function at node i. This local region is fixed until the boundary approaches its limits; then a new narrow band region is defined from the updated signed distance function. However, the signed distance function is only maintained within the narrow band. Thus, before a new region is defined, the implicit function is reinitialized to a signed distance function over the entire design domain to maintain stability. The reinitialization approach adopted in this

DOI: 10.1002/nme

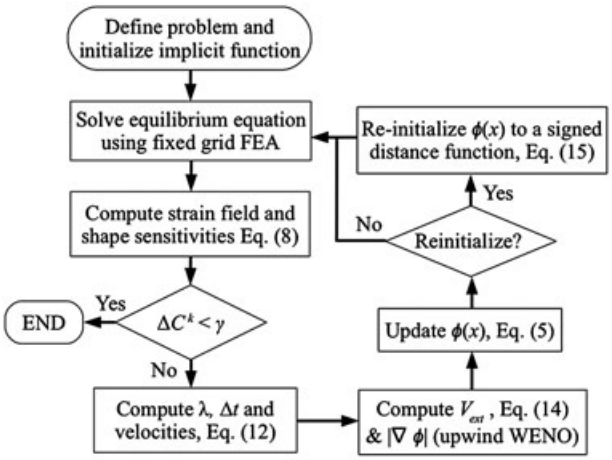

Figure 1. Level set optimization algorithm flowchart.

work is to use the current zero level set as a starting point to solve the eikonal equation using the fast marching method [37]

$$|\nabla \phi| = 1. \tag{15}$$

The upwind finite difference scheme for gradient calculation of ϕ in Equation (5) is often employed by level set methods because of its favorable stability [14]. This scheme is utilized here where each gradient component is approximated using the higher order weighted essentially nonoscillatory method [39] that improves the stability and accuracy of the scheme.

When employing the Lagrange multiplier approach to handle the volume constraint, a fixed value of λ can be used [13]; however, this does not necessarily guarantee constraint satisfaction. An alternative is to compute λ each iteration, assuming the volume of the structure is conserved during boundary propagation [12]. However, this approach can encounter difficulties because preserving volume or mass using the level set method can be problematic [40]. We introduce a robust approach for handling the volume constraint by using an algorithm to compute a λ value that exactly satisfies the constraint each iteration. Because we found the relationship between λ and volume change is often approximately linear, the value of λ is efficiently calculated at each iteration using Newton's method and a numerical approximation for the boundary integral that defines volume change.

A simple termination criterion is employed, based on the maximum change in objective function over the previous 10 iterations

$$\Delta C^k = \frac{\left(C^m_{\max} - C^m_{\min}\right)}{\left(C^m_{\max} + C^m_{\min}\right)},\ m \in [k-9, k], \tag{16}$$

where C^k is the compliance computed at iteration k and the optimization process is stopped if $\Delta C^k < \gamma$, where γ is a small positive number. The algorithm used to solve the minimization of compliance problem, Equation (2), is illustrated in Figure 1.

4. HOLE INSERTION METHOD

4.1. Concept overview

It has been observed that new holes can emerge naturally in 3D problems when two zero level set surfaces cross without breaking the connectivity of the shape or void. It is proposed to exploit this phenomenon to facilitate natural hole creation in 2D problems. To mimic the hole insertion mechanism that occurs in 3D problems, a secondary implicit level set function is introduced, $\bar{\phi}(x)$, to represent a pseudo-third-dimension for the 2D continuum. The pseudo-third-dimension acts

DOI: 10.1002/nme

as a fictitious thickness for the 2D structure. However, it is assumed that the thickness is sufficiently small compared with the dimensions of the 2D structure, allowing thickness effects to be ignored. The secondary implicit level set function is initialized to an artificial height, $\bar{h}$ above the structure domain

$$\bar{\phi}^0(x) = \begin{cases} +\bar{h}, & x \in \Omega_S \\ -\bar{h}, & x \notin \Omega_S \end{cases}. \tag{17}$$

The values of the initialization also define the upper and lower bounds of the secondary implicit function: $-\bar{h} \leqslant \bar{\phi}(x) \leqslant \bar{h}$. An update of the secondary implicit function during each iteration of the optimization is performed in a similar manner as the primary level set function, Equation (5)

$$\bar{\phi}_i^{k+1} = \bar{\phi}_i^k - \Delta t \bar{V}_{n,i}, \tag{18}$$

where velocity values are computed at internal nodes from sensitivity values in the same manner as boundary velocities

$$\bar{V}_n = \bar{\lambda} - \bar{\varsigma}(u), \tag{19}$$

where $\bar{\varsigma}(u)$ is the sensitivity used to update the secondary implicit function.

The link between the shape and topological updates are established by using the same shape sensitivity for the primary level set function as the secondary function, $\bar{\varsigma}(u) = \varsigma(u)$. This completes the analogy of the emergence of a hole as shape optimization in 3D. This is also consistent with the basis of existing methods that identify that the shape and topological derivatives are proportional to each other [23, 30]. However, the key difference in this method is that a hole is created only when it is more optimal to do so compared with updating the existing boundaries.

The consistent definition of sensitivities for the update of both implicit functions forms a meaningful link between boundary shape optimization and topological optimization via new hole creation. This link is further strengthened by using a consistent velocity function definition by setting $\bar{\lambda} = \lambda$ in Equation (19). Using the same Lagrange multiplier in both velocity functions ensures that the algorithm treats both aspects of the optimization, shape of the boundary and topology, equally. Therefore, this approach allows the objective to progress smoothly to an optimum solution, because the holes will only appear when favourable compared with boundary shape optimization. This is demonstrated with the numerical examples in Section 5.

A new hole is created when $\bar{\phi}(x)$ becomes negative within the region of Ω_S, and the new hole is added to the primary level set function by simply copying $\bar{\phi}(x)$onto $\phi(x)$ within Ω_S. The progression of the secondary implicit function is linked to the primary one by using a common value for Δt in Equations (5) and (18) and a consistent velocity definition by setting $\bar{\lambda} = \lambda$ in Equation (19) and by using the same sensitivity definition. Therefore, shape and topology optimization is inherently connected and holes are created when they are beneficial compared with boundary shape optimization. Figure 2 shows an illustration of the proposed hole insertion method.

The optimization could be performed entirely with the secondary implicit function. However, the evolution of the primary implicit function through the level set method promotes stability and smoothness of the boundary during the optimization. Therefore, the primary implicit function is used to produce a smooth and optimal boundary for the structure, whereas the secondary function is used to optimize the topology of the structure.

4.2. Numerical implementation

In practice some care is required when utilizing the secondary implicit function as a device for new hole insertion. First, the choice of the initial artificial height, $\bar{h}$ in Equation (17) affects the ease and frequency that holes can emerge. A larger value of $\bar{h}$ represents a thicker structure causing holes to emerge more gradually, whereas a smaller $\bar{h}$ value allows holes to emerge more frequently.

In the narrow band region, the primary implicit function is updated using extension velocities derived from boundary movement. Therefore, the implicit function value may be updated by either the primary or secondary implicit function within the narrow band. This choice of update is removed

DOI: 10.1002/nme

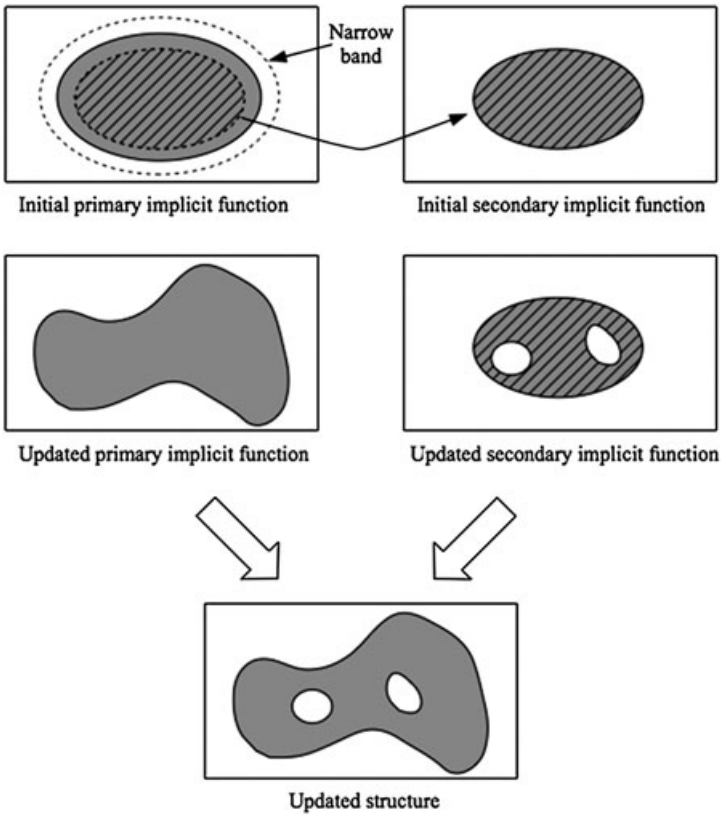

Figure 2. Overview of hole insertion method using two implicit functions.

by limiting hole insertion to the part of Ω_S that is not part of the narrow band region, as shown in Figure 2.

The primary implicit level set function is unlikely to remain a signed distance function when a new hole is created, because values are simply copied from the secondary function. Thus, gradients of the primary implicit function may become too flat or steep around newly created holes, which can adversely affect the stability of the method. This is avoided by reinitializing the primary implicit function to be a signed distance function after a new hole is inserted. It was also found beneficial to reinitialize the secondary implicit function using Equation (17), whenever the primary function is reinitialized.

The velocity function used to update the secondary implicit function, Equation (19), is based on the derivative of the objective function. Therefore, the emergence of new holes through secondary implicit function update is similar to the gradient descent method. Hence, a move limit is introduced to prevent large steps occurring during optimization. A limit, β is applied to the maximum volume of material removed from the structure when new holes are inserted. If this limit is exceeded, then the value of $\bar{\lambda}$ is recomputed so that the limit is satisfied. This computation is performed iteratively using a numerical estimate on new hole volume.

The volume of material removed because of hole insertion is numerically estimated for a trial value of $\bar{\lambda}$. First, a temporary updated secondary implicit function, $\bar{\phi}_{\mathrm{t}}$ is computed using Equations (18) and (19) and the trial value of $\bar{\lambda}$. If no value of $\bar{\phi}_{\mathrm{t}}$ within the structure becomes negative then no new holes are created and $\bar{\phi}_{\mathrm{t}}$ becomes the updated secondary implicit function. Otherwise, the new hole volume is computed by summing volume estimates from each node with a negative $\bar{\phi}_{\mathrm{t}}$ value that lies within the structure, but outside the narrow band, using neighboring values, Figure 3.

To improve the stability of the method, it was found necessary to prevent very small holes being created. A small hole is identified if the four neighboring $\bar{\phi}_{\mathrm{t}}$ values to a node with negative $\bar{\phi}_{\mathrm{t}}$ are all positive. If this occurs then small hole creation is prevented at the node by assigning a small

DOI: 10.1002/nme

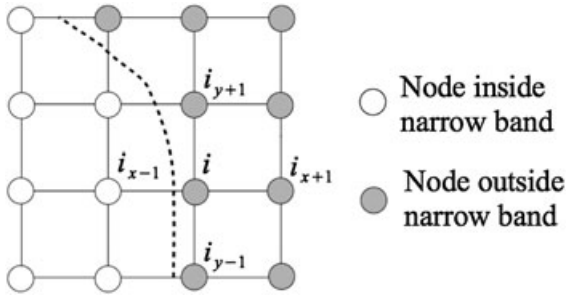

Figure 3. Hole volume estimate for a node near the narrow band region.

positive $\bar{\phi}_{\mathrm{t}}$ value. This ensures that the size of the initial hole is greater than a single element. Once this check has been performed, new hole volume around a node, i is estimated using

$$Vol_i = 0.25h^2 \sum\nolimits_j \Phi_i\left(\bar{\phi}_{t,j}\right),\ \ j \in \left[i_{x-1}, i_{x+1}, i_{y-1}, i_{y+1}\right], \tag{20}$$

where $\Phi_i\left(\bar{\phi}_{t,j}\right)$ is defined by

$$\Phi_i\left(\bar{\phi}_{\mathrm{t},j}\right) = \begin{cases} \bar{\phi}_{\mathrm{t},i} \,/\left(\bar{\phi}_{\mathrm{t},i} - \bar{\phi}_{\mathrm{t},j}\right) & ,\text{if } \ \bar{\phi}_{\mathrm{t},j} \geq 0 \\ 1 & ,\text{if } \ \bar{\phi}_{\mathrm{t},j} < 0 \end{cases}. \tag{21}$$

However, the secondary function is not copied onto the narrow band region of the primary function. Thus, the value for $\bar{\phi}_{\mathrm{t},j}$ used in Equation (21) for nodes inside the narrow band is the current primary function value.

If the new hole volume estimated by summing values computed using Equation (20) for $\bar{\phi}_{\mathrm{t}}$ with $\bar{\lambda} = \lambda$ is greater than the limit, then $\bar{\lambda}$ is modified to meet the limit using Newton's method. The

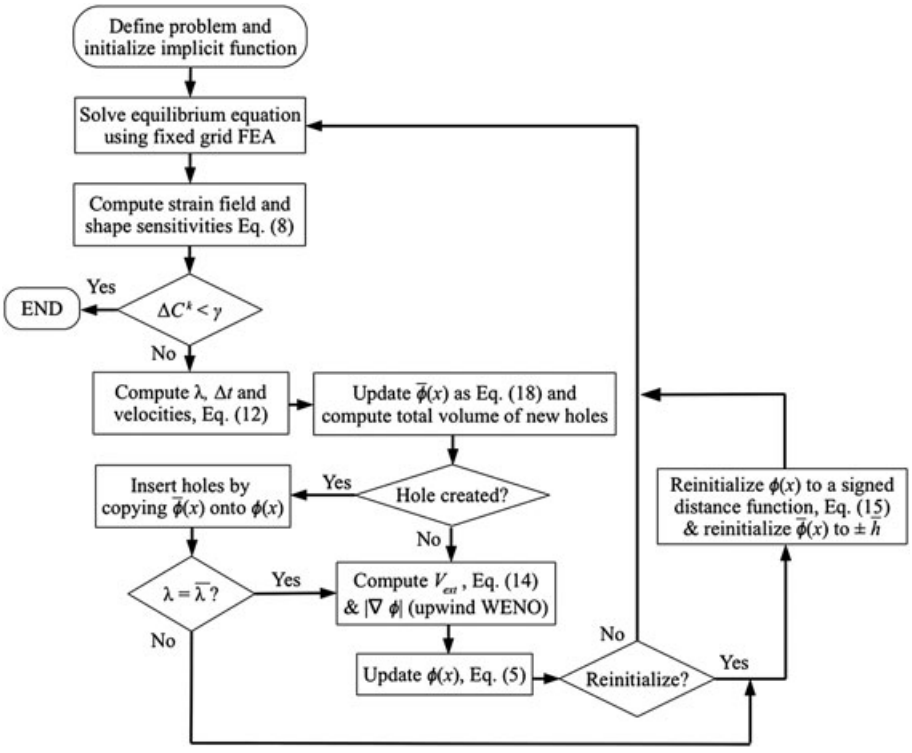

Figure 4. Level set optimization algorithm flowchart with hole insertion.

DOI: 10.1002/nme

iterative Newton's method is terminated when a new hole volume estimate is within 1% of the limit value.

If $\bar{\lambda}$ is modified to meet the new hole volume limit, so that $\bar{\lambda} \neq \lambda$, then the link between primary and secondary function update is invalidated. Thus, primary function update by boundary propagation, Equation (5), is not performed if $\bar{\lambda} \neq \lambda$. Normally, if $\bar{\lambda} = \lambda$, then both hole insertion and boundary propagation can be performed during the same iteration. The complete set optimization algorithm, with the new hole creation method, is illustrated in Figure 4.

5. PARAMETER INVESTIGATIONS

We investigate the numerical parameters and their influences on optimization. These parameters are: narrow bandwidth, ω, new hole volume limit, β, and initial artificial height, $\bar{h}$. Bandwidth and artificial height are defined in terms of the element edge length, h and hole volume limit is defined as a percentage of the current structure volume. The effects of these parameters are investigated using numerical examples to identify suitable values that generally produce good results.

5.1. Cantilever beam

A cantilever beam with aspect ratio 2 : 1 is used for the investigation, Figure 5. The material properties are 1.0 and 0.3 for Young's modulus and Poisson's ratio, respectively. The design domain is discretized using 160 × 80 unit sized ($h = 1$) square elements and the volume constraint is set to 50% of the design domain.

Figure 5. Cantilever beam 2 : 1, initial design and boundary conditions.

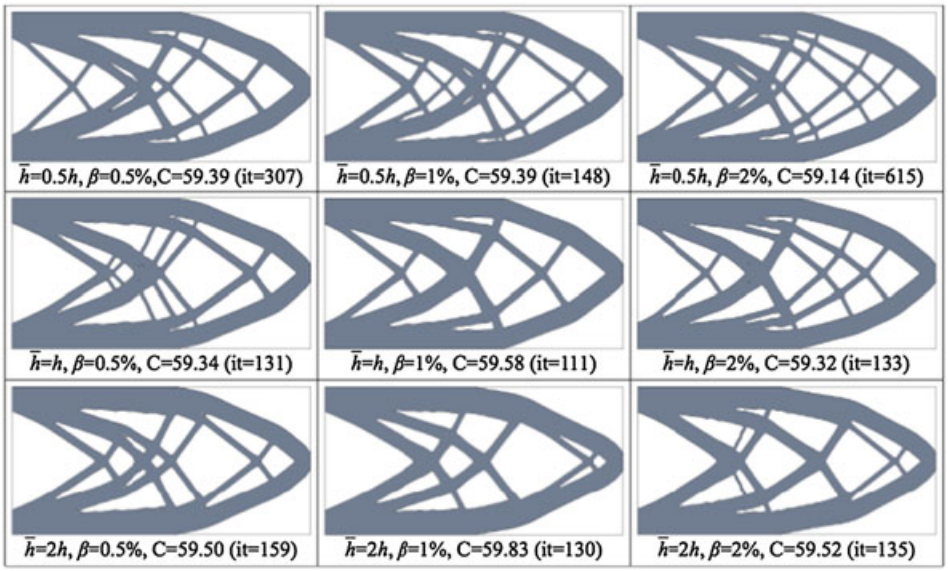

Figure 6. Cantilever beam solutions for band width, $\omega = 4h$. Compliance values, $(C, \times 10^2)$ are for final solution at the iteration (it) shown.

DOI: 10.1002/nme

A range of values are chosen for each parameter: $\bar{h} = 0.5h, h, 2h$; $\beta = 0.5\%, 1\%, 2\%$ of Ω_S; $\omega = 4h, 6h$. The minimization of compliance problem, Equation (2), is solved using the new hole insertion optimization method, Figure 4, for each combination of parameter values. This produces a range of solutions, which are summarised in Figure 6 ($\omega = 4h$) and Figure 7 ($\omega = 6h$). The termination criterion, $\gamma = 0.5 \times 10^{-3}$ was used for all problems.

The results of the investigation show that the solution topologies are dependent on the parameter values. However, the general shape and topology of the structures is reasonably similar and the objective function values of all solutions are within around 1%. This suggests that solutions are not significantly affected by the chosen parameters and the proposed method consistently finds the topological solutions with equivalent performance in practice. However, some generalisations on the effect of each parameter may be drawn from this example.

In general, the larger bandwidth, $\omega = 6h$ produces solutions with more consistent shape and topology that converge in fewer iterations compared with $\omega = 4h$. Because hole insertion is prohibited inside the bandwidth, a larger bandwidth prevents holes being inserted close to each other. This attribute of larger bandwidths thus has an effect of precluding numerical errors near boundaries or in narrow regions between two boundaries and allows the optimization to progress more smoothly. Lower values of the artificial height, $\bar{h}$ allow new holes to emerge more frequently during optimization and, as a consequence, solutions obtained with lower values tend to possess more holes than solutions obtained using higher $\bar{h}$ values. Also, smaller values for the new hole volume limit, β were active more often during optimization iterations than larger values. Furthermore, the largest limit considered, $\beta = 2\%$ was often only active once or twice during optimization and not active at all for $\omega = 6h, \bar{h} = 1.0$. Therefore, a larger limit on new hole volume is less likely to disrupt the optimization by having to modify the $\bar{\lambda}$ value, which prevents update by boundary propagation. However, a limit is still required to prevent too much material being removed in a single iteration.

5.2. *Simply-supported beams*

The parameter investigation was repeated for two further examples, giving a total of 54 cases, and similar results were obtained. Therefore, complete results of these additional investigations are omitted for brevity. The overall results suggest that using a bandwidth, $\omega = 6h$, artificial height,

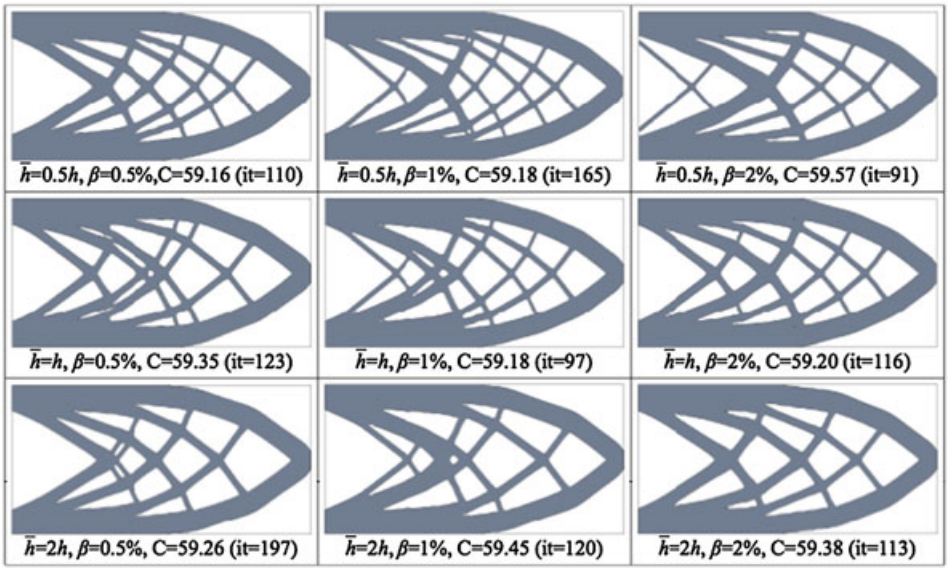

Figure 7. Cantilever beam solutions for bandwidth, $\omega = 6h$. Compliance values, $(C, \times 10^2)$ are for final solution at the iteration (*it*) shown.

DOI: 10.1002/nme

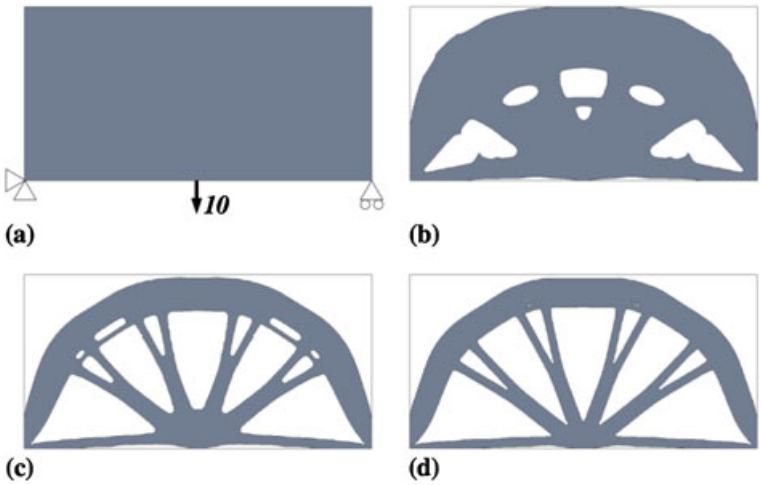

Figure 8. Michell structure: (a) initial design and boundary conditions; (b) design after 35 iterations; (c) 70 iterations; and (d) converged solution after 107 iterations.

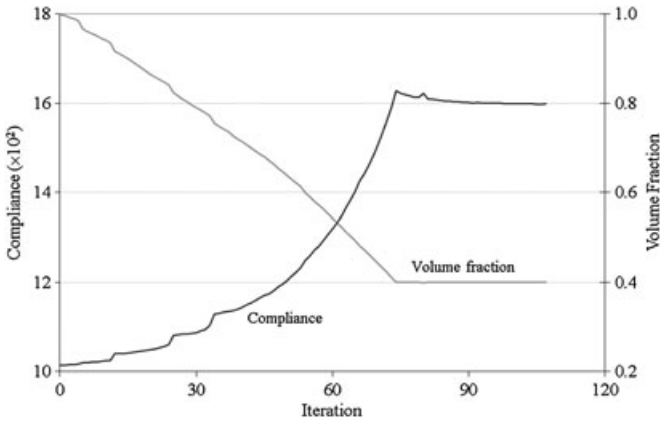

Figure 9. Michell structure, convergence history.

$\bar{h} = h$ and volume limit, $\beta = 2\%$ usually achieves smooth convergence often with fewer iterations. In our experience we observe this finding to be generally applicable to a wider range of optimization problems.

The results for the two additional examples using the recommended parameter values are presented for demonstration. The material properties for both examples are 1.0 and 0.3 for Young's modulus and Poisson's ratio, respectively, and the termination criterion is $\gamma = 0.5 \times 10^{-3}$. The first example is a Michell type structure, Figure 8(a), discretized using 160×80 unit sized square elements and the volume constraint is set to 40% of the design domain. The convergence history for this example is shown in Figure 9.

The second additional example is a Messerschmitt-Bölkow-Blohm (MBB). Using symmetry conditions about the vertical axis, only the right half of the beam is considered, Figure 10(a). The design domain is discretized using 180×60 unit sized square elements and the volume constraint is set to 40%. The convergence history is shown in Figure 11.

The numerical investigation allowed for some general observations on the performance of the algorithm. First, examples exhibit reasonably smooth convergence with no significant oscillations or discontinuities in compliance. A smoother convergence is more evident with an increasing bandwidth, for example, $\omega = 6h$. A close examination of the topological changes does not show holes disappearing immediately after creation or significant movement of newly created holes. This supports that the link between hole insertion and boundary propagation, created through a consistent

DOI: 10.1002/nme

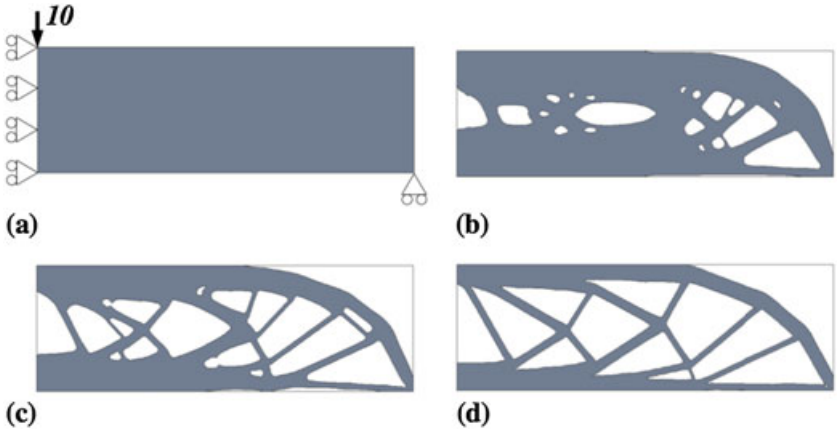

Figure 10. MBB beam: (a) initial design and boundary conditions; (b) design after 30 iterations; (c) 50 iterations; and (d) converged solution after 109 iterations.

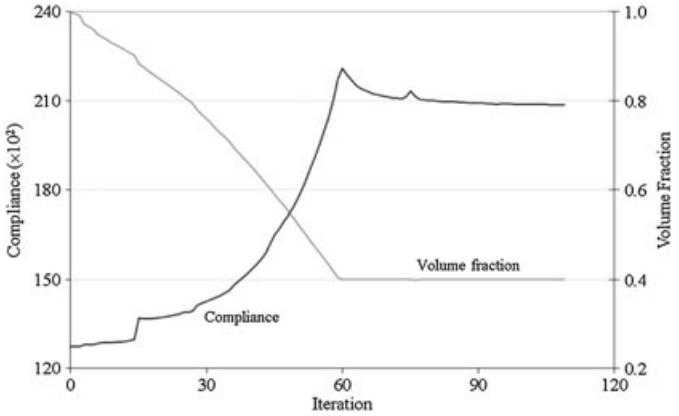

Figure 11. MBB beam, convergence history.

velocity function definition for the update of both implicit functions, is maintained throughout the optimization. The step-increases in the compliance value observed in the early stages of optimization coincide with the insertion of new holes when the new hole volume limit is active, Figures 9 and 11. In these incidences, the $\bar{\lambda}$ value is modified, but the topological evolutions do not show disruptions or sudden changes. Once the volume constraint is satisfied (around iteration 70 in Figure 9 and iteration 60 in Figure 11), compliance is minimised while maintaining the volume and the small peaks in compliance coincide with topological changes where thin bars are eliminated because the mesh size cannot represent them.

Most new holes are inserted during the initial stages of the optimization, before the volume constraint is reached. This is shown in the intermediate designs for the Michell structure, Figures 8(b) and (c), and MBB, Figures 10(b) and (c). After the constraint is reached, often only a few iterations are required to obtain the final solution. This suggests that new holes are created in optimal locations and are retained in the final solution.

6. FURTHER NUMERICAL EXAMPLES

6.1. Cantilever beam with different initial designs

The cantilever beam example, Figure 5, is optimized again using different initial designs with and without hole insertion. Three different initial designs are chosen and the solutions obtained are shown in Figure 12. The convergence criterion for all solutions is $\gamma = 10^{-3}$.

DOI: 10.1002/nme

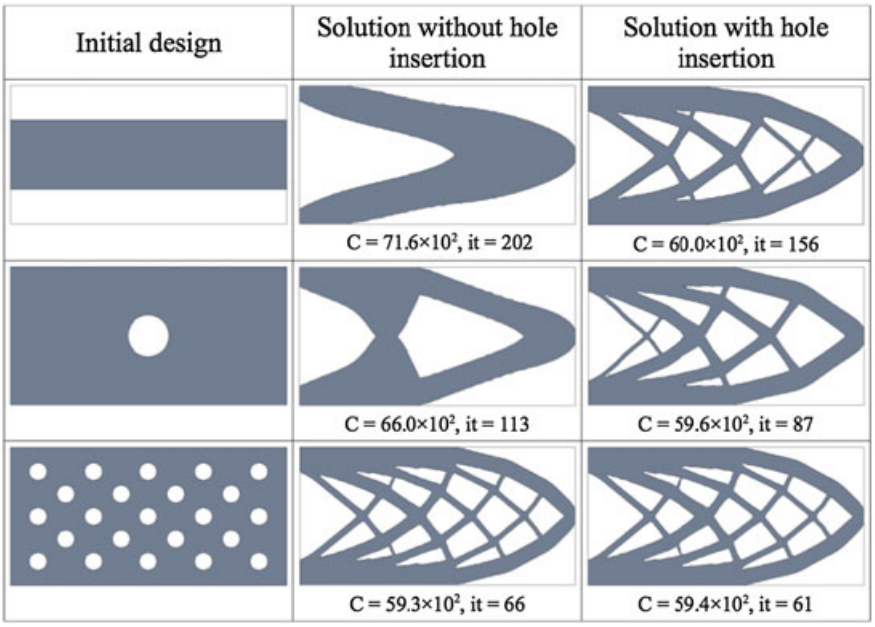

Figure 12. Cantilever solutions with different initial designs. Compliance values, (C) are for final solutions at the iteration (it) shown.

As expected, solutions obtained without the hole insertion method are highly dependent on the initial design and there is a difference of up to 20% in final compliance values. In contrast, solutions obtained with hole insertion are more consistent and there is only about a 1% difference in the final compliance values, Figure 12. This demonstrates that the proposed hole insertion method reduces the dependency on the initial design, thus improving the reliability of the direct level set optimization method.

6.2. *Multiple load cases*

This section employs the level set method with the proposed hole insertion method to solve a minimization of compliance problem subject to multiple load cases. First, the multiple load case problem is stated as

$$\begin{aligned} &\text{Minimize:} C(u,\phi) = \sum_{i=1}^{m} w_i \int_{\Omega} E\varepsilon(u_i)\varepsilon(u_i)H(\phi)\mathrm{d}\Omega \\ &\text{Subject to:} \int_{\Omega} H(\phi)\mathrm{d}\Omega \leqslant Vol^* \end{aligned} \quad , \tag{22}$$

where m is the number of separate load cases and w_i is the weight for load case i. If there are no body forces, then u_i is the solution to the following static equilibrium equation:

$$\int_{\Omega} E\varepsilon(u_i)\varepsilon(v)H(\phi)\,\mathrm{d}\Omega = \int_{\Gamma_S} f_i v \mathrm{d}\Gamma_S \ , \quad u_i|_{\Gamma_D} = 0 \ \ \forall v \in U. \tag{23}$$

The shape sensitivity for the multiple load case problem, ς_m can be derived as [41]

$$\varsigma_m = \sum_{i=1}^{m} w_i E\varepsilon(u_i)\varepsilon(u_i). \tag{24}$$

This shape sensitivity can be used to construct velocity functions for the primary and secondary implicit function update in the same fashion as the single load case problem, Equations (12) and (19), respectively.

DOI: 10.1002/nme

A beam with multiple load cases is optimized using the new hole insertion method. The beam is shown in Figure 13(a) and has three load cases, f_i, spaced equally along the bottom edge. Each load case has a magnitude of 2.0 and a weight of 1.0. The material properties are 1.0 and 0.3 for Young's modulus and Poisson's ratio, respectively, and the termination criterion is $\gamma = 0.5 \times 10^{-3}$. The beam is discretized using 200×50 unit-sized square elements and the volume constraint is set to 40% of the design domain. The convergence history for this example is shown in Figure 14.

The multiple load case beam converges to a solution after 144 iterations with a total compliance value of 4.67×10^2, Figure 13(d). This solution is in good agreement with that obtained using an element based method [1]. The convergence of the objective function (Figure 14) again shows a smooth optimization, with a few jumps early in the optimization because of hole insertion. This

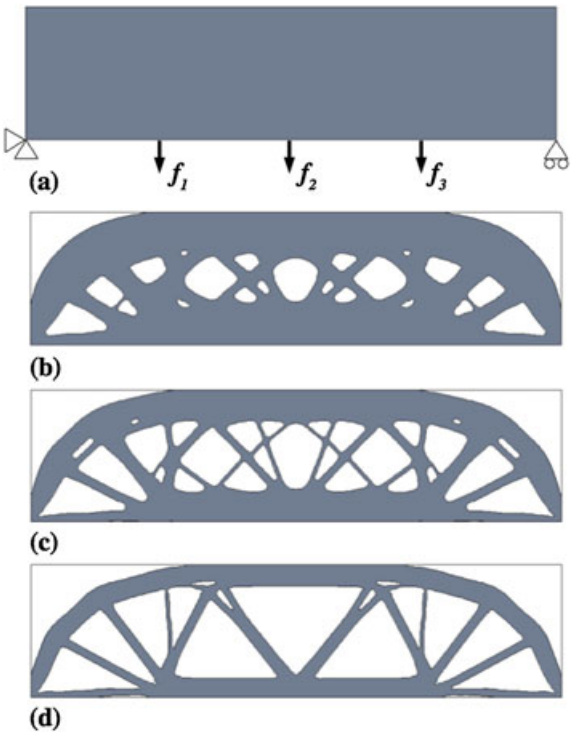

Figure 13. Beam optimization for multiple load cases: (a) initial design and boundary conditions; (b) design after 25 iterations; (c) 40 iterations; and (d) converged solution after 144 iterations.

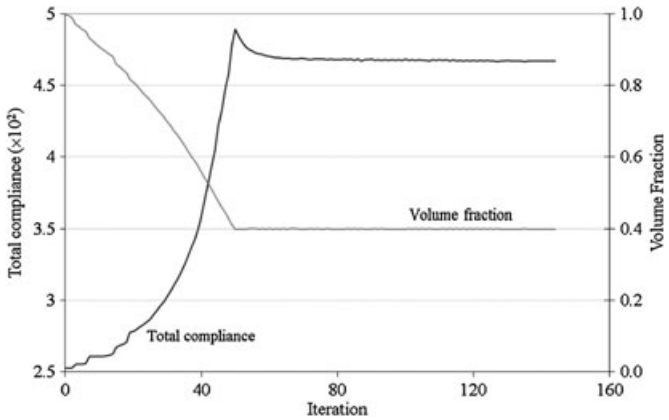

Figure 14. Beam optimization for multiple load cases, convergence history.

DOI: 10.1002/nme

demonstrates that the proposed hole insertion method can obtain a good solution for a multiple load case problem.

The examples presented here are all two-dimensional and the secondary implicit function can be thought of as describing the thickness of the structure in a third dimension. However, this concept can easily be extended to allow hole insertion for three-dimensional problems, although the physical analogy of the secondary implicit function becomes obscure.

7. CONCLUSIONS

In this paper a new technique for inserting holes when using the direct level set based topology optimization method is presented and investigated. Holes are allowed to emerge through update of a secondary implicit level set function that describes a pseudo-thickness of a two-dimensional structure. The update of the secondary function is linked to the primary level set function using common values for the time step and volume constraint Lagrange multiplier and the velocity function is defined using the same shape sensitivity definition. This approach provides a meaningful link between boundary propagation and creation of new holes and achieves smooth convergence to optimum solutions.

Investigations using classic minimization of compliance problems show that solutions are not significantly affected by the choice of parameters. However, a suitable set of parameters is indentified that provide good solutions to the problems considered. It is also observed that most holes emerge during the early stages and are often retained in the final solution, suggesting that holes are created in optimal locations. Overall, the new hole insertion method is able to smoothly obtain optimum solutions for a range of examples and is not significantly sensitive to the choice parameters or the initial design.

ACKNOWLEDGEMENTS

The work reported in this paper has been undertaken as part of the UK Engineering and Physical Sciences Research Council funded Innovative Design and Manufacturing Research Centre at the University of Bath. The authors would also like to thank Numerical Analysis group at the Rutherford Appleton Lab for their FORTRAN HSL packages.

REFERENCES

1. Bendsøe MP, Sigmund O. *Topology optimization: Theory, Methods and Applications*. Springer-Verlag: Germany, 2004.
2. Rozvany G. Aims, scope, methods, history and unified terminology of computer-aided topology optimization in structural mechanics. *Structural and Multidisciplinary Optimization* 2001; **21**(2):90–108.
3. Diaz A, Sigmund O. Checkerboard patterns in layout optimization. *Structural Optimization* 1995; **10**(1):40–45.
4. Jog CS, Haber RB. Stability of finite element models for distributed-parameter optimization and topology design. *Computer Methods in Applied Mechanics and Engineering* 1996; **130**(3-4):203–226.
5. Haber RB, Jog CS, Bendsøe MP. A new approach to variable-topology shape design using a constraint on perimeter. *Structural Optimization* 1996; **11**(1):1–12.
6. Sigmund O, Petersson J. Numerical instabilities in topology optimization: A survey on procedures dealing with checkerboards, mesh-dependencies and local minima. *Structural Optimization* 1998; **16**(1):68–75.
7. Tang PS, Chang KH. Integration of topology and shape optimization for design of structural components. *Structural and Multidisciplinary Optimization* 2001; **22**(1):65–82.
8. Hsu YL, Hsu MS, Chen CT. Interpreting results from topology optimization using density contours. *Computers and Structures* 2001; **79**(8):1049–1058.
9. Kim H, Querin OM, Steven GP, Xie YM. Improving efficiency of evolutionary structural optimisation by implementing fixed grid mesh. *Structural and Multidisciplinary Optimization* 2002; **24**(6):441–448.
10. Eschenauer HA, Kobelev VV, Schumacher A. Bubble method for topology and shape optimization of structures. *Structural Optimization* 1994; **8**(1):42–51.
11. Lee S, Kwak BM, Kim IY. Smooth boundary topology optimization using b-spline and hole generation. *International Journal of CAD/CAM* 2007; **7**(1):1–16.
12. Wang MY, Wang X, Guo D. A level set method for structural topology optimization. *Computer Methods In Applied Mechanics and Engineering* 2003; **192**(1-2):227–246.

DOI: 10.1002/nme

13. Allaire G, Jouve F, Toader AM. Structural optimization using sensitivity analysis and a level-set method. *Journal of Computational Physics* 2004; **194**(1):363–393.
14. Sethian JA. *Level set methods and fast marching methods*, 2nd edn. Cambridge University Press: New York, 1999.
15. Osher S, Fedkiw R. *Level set methods and dynamic implicit surfaces*. Springer: New York, 2003.
16. Burger M, Hackl B, Ring W. Incorporating topological derivatives into level set methods. *Journal of Computational Physics* 2004; **194**(1):344–362.
17. He L, Kao C-Y, Osher S. Incorporating topological derivatives into shape derivatives based level set methods. *Journal of Computational Physics* 2007; **225**(1):891–909.
18. Amstutz S, Andra H. A new algorithm for topology optimization using a level-set method. *Journal of Computational Physics* 2006; **216**(2):573–588.
19. Norato JA, Bendsøe MP, Haber RB, Tortorelli DA. A topological derivative method for topology optimization. *Structural and Multidisciplinary Optimization* 2007; **33**(4-5):375–386.
20. Allaire G, de Gournay F, Jouve F, Toader AM. Structural optimization using topological and shape sensitivity via a level set method. *Control and Cybernetics* 2005; **34**(1):59–80.
21. Belytschko T, Xiao SP, Parimi C. Topology optimization with implicit functions and regularization. *International Journal for Numerical Methods in Engineering* 2003; **57**(6):1177–1196.
22. Sethian J, Wiegmann A. Structural boundary design via level set and immersed interface methods. *Journal of Computational Physics* 2000; **163**(2):489–528.
23. Park K-S, Youn S-K. Topology optimization of shell structures using adaptive inner-front (AIF) level set method. *Structural and Multidisciplinary Optimization* 2008; **36**(1):43–58.
24. Yamada T, Izui K, Nishiwaki S, Takezawa A. A Topology Optimization Method Based on the Level Set Method Incorporating a Fictitious Interface Energy. *Computer Methods in Applied Mechanical Engineering* 2010; **199**:2876–2891.
25. Wang SY, Lim KM, Khoo BC, Wang MY. On Hole Nucleation in Topology Optimization Using the Level Set Methods. *CMES-Computer Modeling In Engineering & Sciences* 2007; **21**:219–238.
26. Wang SY, Wang MY. Radial basis functions and level set method for structural topology optimization. *International Journal for Numerical Methods in Engineering* 2006; **65**(12):2060–2090.
27. Luo Z, Tong L. A level set method for shape and topology optimization of large-displacement compliant mechanisms. *International Journal for Numerical Methods in Engineering* 2008; **76**(6):862–892.
28. Gomes AA, Suleman A. Application of spectral level set methodology in topology optimization. *Structural and Multidisciplinary Optimization* 2006; **31**(6):430–443.
29. Chen J, Zhao D, Huang Z, Zheng Y, Gao S. Evolutionary level set method for structural topology optimization. *Computers & Structures* 2011; **89**:445–454.
30. Céa J, Garreau S, Guillaume P, Masmoudi M. The shape and topological optimizations connection. *Computer Methods in Applied Mechanics and Engineering* 2000; **188**(4):713–726.
31. Cook RD, Malkus DS, Plesha ME, Witt RJ. *Concepts and applications of finite element analysis*, 4th edn. Wiley: United States, 2002.
32. Jang G-W, Kim YY, Choi KK. Remesh-free shape optimization using the wavelet-galerkin method. *International Journal of Solids and Structures* 2004; **41**(22-23):6465–6483.
33. Wang SY, Wang MY. A moving superimposed finite element method for structural topology optimization. *International Journal for Numerical Methods in Engineering* 2006; **65**(11):1892–1922.
34. Liu Z, Korvink JG, Huang R. Structure topology optimization: fully coupled level set method via FEMLAB. *Structural and Multidisciplinary Optimization* 2005; **29**(6):407–417.
35. Wei P, Wang MY, Xing X. A study on x-fem in continuum structural optimization using a level set model. *Computer-Aided Design* 2010; **42**(8):708–719.
36. Dunning PD, Kim HA, Mullineux G. Investigation and improvement of sensitivity computation using the area-fraction weighted fixed grid FEM and structural optimization. *Finite Elements in Analysis and Design* 2011; **47**:933–941.
37. Adalsteinsson D, Sethian JA. The fast construction of extension velocities in level set methods. *Journal of Computational Physics* 1999; **148**(1):2–22.
38. Adalsteinsson D, Sethian JA. A fast level set method for propagating interfaces. *Journal of Computational Physics* 1995; **118**(2):269–277.
39. Jiang G-S, Peng D. Weighted ENO schemes for hamilton-jacobi equations. *SIAM Journal on Scientific Computing* 2000; **21**(6):2126–2143.
40. Wang SY, Lim KM, Khoo BC, Wang MY. An extended level set method for shape and topology optimization. *Journal of Computational Physics* 2007; **221**(1):395–421.
41. Allaire G, Jouve F. A level-set method for vibration and multiple loads structural optimization. *Computer Methods In Applied Mechanics and Engineering* 2005; **194**(30-33):3269–3290.

DOI: 10.1002/nme